Quantitative Measurements and Modeling of Kinetics in Nucleic Acid Monolayer Films Using SPR Spectroscopy

R. Georgiadis,* K. P. Peterlinz, and A. W. Peterson

Contribution from the Department of Chemistry, Boston University, 590 Commonwealth, Boston, Massachusetts 02215

Received August 24, 1999

Abstract: We report a quantitative study of the kinetics of formation for a two-component tethered ssDNA monolayer film using *in situ* two-color surface plasmon resonance (SPR) spectroscopy. The attachment of the DNA to gold is facilitated by functionalization at the 5′ end with a thiol group connected by a hexamethylene linker (HS-C6-ssDNA). Detailed data analysis is performed by quantitative comparison of the DNA coverage versus time kinetic data obtained from SPRS with numerical solutions for the differential equations for simultaneous adsorption, desorption, and diffusion at the interface. The kinetics of adsorption of HS-C_6-ssDNA onto bare gold as well as the kinetics of loss of HS-C_6-ssDNA from the surface during subsequent treatment with mercaptohexanol can be understood in terms of a simple physical model and self-consistent parameters. The kinetics of HS-C_6-ssDNA adsorption on bare gold are compared to the kinetics of hybridization of surface-attached thiolated ssDNA with the fully complementary ssDNA in free solution and found to follow remarkably similar kinetic pathways. In contrast, the adsorption of ssDNA follows complex kinetics that cannot be modeled with a single kinetic step. That is, the presence of a thiol functionality on a 25-mer ssDNA gives rise to adsorption behavior that is clearly kinetically distinct from simple ssDNA adsorption on gold.

1. Introduction

The interaction between DNA-functionalized surfaces and free oligonucleotides in solution is the key to a wide range of new genetic diagnostic devices.[1] These devices, which rely on the binding of analyte nucleic acids to surface-tethered DNA strands, show great promise in a range of medical, pharmaceutical, and forensic applications.[2] However, the nature of the interactions between probe and target remains only partially characterized as there have been few systematic studies.[1] For example, dramatic differences in duplex yield are not due to differences in overall stability of duplexes but rather due to different rates of forward reaction.

Optical surface plasmon resonance spectroscopy (SPRS) is a powerful tool for *in situ* real-time characterization of solid/liquid interfaces. In the past decade, SPRS has found increasingly widespread use for the study of interactions of biological molecules in so-called optical biosensors.[3] The power of the optical biosensor experimental approach, in which one of the interacting molecules (the analyte) is free in solution and the other (the ligand) is attached to the biosensor surface, is that the formation and decomposition of the analyte/ligand complex is monitored in situ, yielding kinetic data in real-time. The assembly or binding process can be monitored without the need to label the reactants with spectroscopic or radioactive probes, making this technique an ideal noninvasive in situ method amenable to a wide range of biologically relevant molecules including nucleic acids, proteins, lipids, and carbohydrates.

In principle, the availability of real-time SPRS kinetic data provides the possibility of determining the mechanism of the chemical and/or physical binding event and, using the law of mass action, equilibrium constants for surface reactions. The major obstacle to obtaining accurate and reliable kinetic and thermodynamic information from analysis of kinetic data is the need for very high quality experimental data. Reliable measurements of surface coverage must be available over a wide range of time scales and solution conditions. Moreover, if simple physical models are to be used to describe the data, it is critical that all experimental artifacts be minimized and accounted for.

In practice, the ultimate promise of optical biosensor technology to provide molecular level information regarding bimolecular and biomaterial processes remains elusive. While the development of a number of commercial SPRS instruments has led to an exponential growth of SPR-related publications, kinetic analysis approaches used in many studies have contained fundamental flaws in the equations and assumptions,[4,5] a problem exacerbated by the fact that derived results in many cases seemed of the right order when compared with traditional measurements which have very wide margins of error.[6] In addition, a number of experimental artifacts can complicate interpretation of kinetic data, including nonspecific binding, mass transport, matrix effects associated with heterogeneity, and nonideality in the biosensor interaction region which is often a thick polymer matrix (∼1000 Å).[7] An alternative approach, and the one used here, is to use self-assembled monolayer films directly on gold SPRS sensor surface.[8−10] For this case, signal

(1) Southern, E.; Mir, K.; Shchepinov, M. *Nat. Genet.* **1999**, *21*, 5−9.
(2) Fodor, S. P. A. *Science* **1997**, *277*, 393−395.
(3) Garland, P. B. *Q. Rev. Biophys.* **1996**, *29*, 91−117.
(4) Morton, T. A.; Myszka, D. G. *Methods Enzymol.* **1998**, *295* (Energetics of Biological Macromolecules, Part B, pp 268−294).
(5) Schuck, P. *Current Opinion Biotechnol.* **1997**, *8*, 498−502.
(6) Davies, J. *Surface Analytical Techniques for Probing Biomaterial Processes*; Davies, J., Ed.; CRC Press: Boca Raton, FL, 1996.
(7) Schuck, P. *Biophys. J.* **1996**, *70*, 1230−1249.
(8) Peterlinz, K. A.; Georgiadis, R. *Opt. Commun.* **1996**, *130*, 260−266.
(9) Peterlinz, K. A.; Georgiadis, R. *Langmuir* **1996**, *12*, 4731−40.
(10) Peterlinz, K. A.; Georgiadis, R.; Herne, T. M.; Tarlov, M. J. *J. Am. Chem. Soc.* **1997**, *119*, 3401−2.

10.1021/ja9930824 CCC: $19.00
Published on Web 03/16/2000

levels are generally significantly reduced due to fewer molecules in the interfacial region.

In this paper we have focused on a system involving self-assembled monolayer films on gold surfaces for which the planar geometry of the interface and relatively simple film structure provides a model interface that is tractable to analysis using simple physical models. In addition, the optical measurements are obtained using a two-color SPRS optical technique[8] that provides highly sensitive, quantitative measurements of surface coverage[9,10] even for submonolayer films. The kinetic data are of high quality and can be used to test various proposed kinetic models. In addition to studying both adsorption and desorption steps involved in the process of forming two-component monolayer nucleic acid films via self-assembly, we also examine the kinetics of hybridization when these films are exposed to a nucleic acid of complementary sequence.

In this work, the tailored interfaces are fabricated using molecular self-assembly techniques[11] to covalently tether alkanethiol derivatives of single-stranded DNA oligomers to a gold substrate. The resulting nucleic acid monolayer films have controlled film composition which resists nonspecific binding and maintains a low surface density of ligands.[10] We have shown previously[10] that exposure of these nucleic acid films to a complementary strand of ssDNA leads to highly efficient reversible hybridization as characterized by *in situ* SPRS temperature dependent melting studies with no measurable nonspecific binding. These are important attributes of model biosensor surfaces where, to maintain biochemical function, the optimum mole fraction of the biochemical active molecule in the monolayer film may be quite small. Experiments on model interfaces with such very low surface densities require highly sensitive probes and special attention to the issue of nonspecific adsorption.

Despite the wide-spread use of self-assembly methodologies for fabrication of tailored organic thin films,[12] a detailed understanding of the process by which these films form is still lacking. This knowledge is particularly important for research and applications of mixed multicomponent monolayer films in which the composition of the film determines the physical and chemical properties of the interface. For much of the work on mixed monolayer films, researchers have relied on thermodynamic constraints to control the film composition. However, the final composition of the monolayer film may or may not be similar to the mole fraction of the component molecules in the solution to which the surface is exposed. When the adsorption rates of the component molecules are vastly different, as with large differences in molecular size or with dissimilar surface chemical reaction rates, kinetic constraints will ultimately control film composition so that the solution concentration and other parameters must be tuned for the desired results. Another general approach, and the method used in this work, is to control the film composition by exposing the metal surface for appropriate times to a sequence of solutions with appropriate concentrations. Here again, knowledge of kinetics is needed to deduce appropriate conditions. In either case, issues of segregation and islanding cannot be addressed directly with optical probes; these await the development of nonintrusive nanoscale measurements amenable to real-time kinetic studies. To date, scanning probe methods have begun to address these issues, although with limited success with respect to high-quality kinetic data.[13]

In this paper, we focus mainly on detailed measurements of the sequential kinetic steps that lead to formation of a two-component film which consists of a functionalized 25-mer ssDNA with pendant $(CH_2)_6SH$ at the 5′ position and a diluent mercaptohexanol. The two-color SPRS kinetic data presented here are of sufficient quality that it is possible to unambiguously test detailed kinetic models. We find that, for a diverse range of surface processes, the kinetics cannot be understood without assuming dynamic equilibrium, which includes adsorption to the surface, desorption from the surface, and diffusion at the interface.

2. Materials and Methods

The two-color SPRS apparatus used for measurements presented here has been described previously.[8,10] Surface plasmon resonance spectroscopy is an all-optical technique that is sensitive to changes in the dielectric constant at a metal surface for certain metals such as gold. In an attenuated total reflectance (ATR) SPRS experiment, p-polarized monochromatic light is reflected from a glass prism−metal interface, and the reflectivity of the light is measured as a function of incident angle. At an optimal coupling angle, the evanescent field of the light couples to a plasmon mode that propagates along the metal surface, and a minimum in reflected intensity is observed. For a given frequency of light, the wave vector of the plasmon depends strongly on the dielectric constants of all materials at the interface.[14] In general, the SPR spectrum can be fit to an optical model that accounts for the thickness and complex dielectric constants of all materials at the interface;[9] however, the thickness and dielectric constant for films <200 Å cannot be determined uniquely from a single SPRS measurement.[15] As reported previously, two-color SPRS allows unique determination of both the thickness and dielectric constant of a transparent dielectric film.[8]

For these experiments, the p-polarized output from two He−Ne lasers was used (632.8 and 543.5 nm). The prism material was SF-14 (n = 1.76), and all other components of the liquid cell were either glass, PTFE, or Kalrez. The cell temperature was monitored continuously using a PTFE-lined Chromel-Alumel thermocouple built into the sample cell. The gold substrate was prepared by evaporation of 99.999% purity gold directly onto a hemicylindrical prism which had been previously prepared by exposing the flat face of the prism to a hot (50−70 °C) 30% H_2O_2/70% H_2SO_4 (piranha) solution, rinsing with Nanopure water, drying with nitrogen, and baking overnight in a 120 °C oven. The film was deposited by first evaporating a 12 Å layer of Cr at 1 Å/s, followed by evaporating a ∼500 Å layer of gold at 1.5−2 Å/s. The prism was then sealed with a Kalrez O-ring to a PTFE cell on the surface plasmon resonance (SPR) apparatus. The prism remained sealed to the cell for all experiments, with the lasers focused onto the same spot. Once sealed to the cell, the gold surface was prepared by exposure to room temperature piranha solution for 10 min followed by rinsing with copious quantities of Nanopure water and ethanol. (*CAUTION: Piranha solution can react violently with organic material, and should be handled with extreme caution. Piranha solution should not be stored in tightly sealed containers.*) All water used was Nanopure (18 MΩ/cm). KH_2PO_4 was obtained from Fisher. The mercaptohexanol was kindly provided by Prof. Cary Miller (University of Maryland). The thiol derivatized ssDNA (HS-C_6-ssDNA), underivatized ssDNA, and the underivatized complement (ssDNA complement) were provided by Dr. M. J. Tarlov and co-workers (NIST). The sequence was R-CAC GAC GTT GTA AAA CGA CGG CCA G, where R = HS−$(CH_2)_6$ at the 5′ end. The complementary sequence was GTG CTG CAA CAT TTT GCT GCC GGT C.

The ssDNA tethered films were formed *in situ* on the gold substrate by first exposing the gold surface to a 1 mM solution of the HS-C_6-ssDNA in 1.0 M KH_2PO_4 for about 5 h. After exposure, the cell was

(11) Whitesides, G. M.; Ferguson, G. S.; Allara, D.; Scherson, D.; Speaker, L.; Ulman, A. *Crit. Rev. Surf. Chem.* **1993**, *3*, 49−65.

(12) Mrksich, M.; Whitesides, G. M. *Annu. Rev. Biophys. Biomol. Struct.* **1996**, *25*, 55−78.

(13) Xu, S.; Cruchon-Dupeyrat, S. J. N.; Garno, J. C.; Liu, G.-Y.; Kane Jennings, G.; Yong, T.-H.; Laibinis, P. E. *J. Chem. Phys.* **1998**, *108*, 5002−5012.

(14) Raether, H. *Surface Plasmons, Springer Tracts in Modern Physics*; Springer-Verlag: Berlin, 1988; Vol. 111.

(15) Peterlinz, K. A.; Georgiadis, R. *J. Phys. Chem.* **1997**, *101*, 8041.

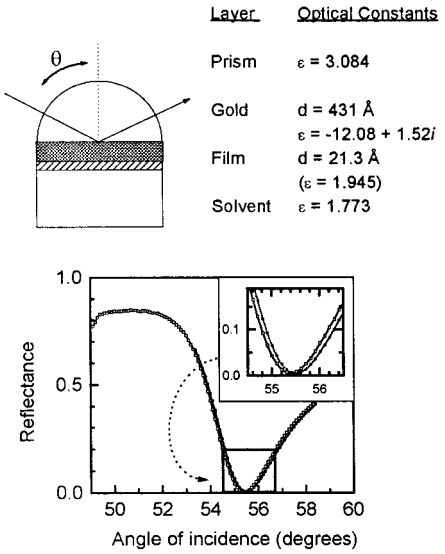

Figure 1. At the top is shown a schematic of the experimental geometry and a list of parameters in the optical layer model of the interface used for analysis of SPR spectroscopy reflectance data in water. At the bottom are shown raw reflectivity data for 632.8 nm excitation for bare gold (open circles) and for gold modified by self-assembly of a monolayer film of thiol derivitized ssDNA (closed circles). Also shown are the best fits to the data (solid and dashed lines) obtained from the optical parameters; see text for details.

rinsed with copious quantities of Nanopure water and then exposed to a 1 mM solution of mercaptohexanol in Nanopure water for about 12 h. The cell was then rinsed with copious quantities of Nanopure water. Hybridization measurements were made using this tethered ssDNA film as described earlier.[10] The ssDNA adsorption on bare gold was measured using a clean, piranha-treated gold substrate.

3. Data Analysis

1. Extraction of Surface Coverage Information from Optical SPRS Measurements. Figure 1 shows a typical SPRS reflectance curve consisting of angle of incidence modulated data obtained at a fixed excitation wavelength. As shown by Raether[14] and others,[16−18] SPR spectra can be fit with an optical model that accounts for the thickness, d_f, and dielectric constant, ϵ_f, of an adsorbed thin film. Typically, the calculated reflectivity function uses Fresnel equations for a four-layer model (prism/metal/film/liquid) to extract the values of the two unknown thin-film parameters (d_f and ϵ_f) assuming that the thicknesses and complex dielectric constants of the prism, metal, and other materials near or in contact with the metal surface are known or can be obtained from control experiments. Figure 1 gives the parameter values used in the optical layer model to calculate the reflectance spectrum shown.

For very thin films <200 Å, any number of combinations of d_f *and* ϵ_f may be found to fit a single reflectance curve. Consequently, thin-film thicknesses, d_f, determined in this way from a single wavelength measurement will have high uncertainty without independent a priori knowledge of ϵ_f.[8,15,19] Most researchers resort to assuming a fixed value for the film dielectric constant based on the chemical properties of the neat film material. This method can provide relative thickness information from SPR spectra, but cannot provide quantitative surface coverage.

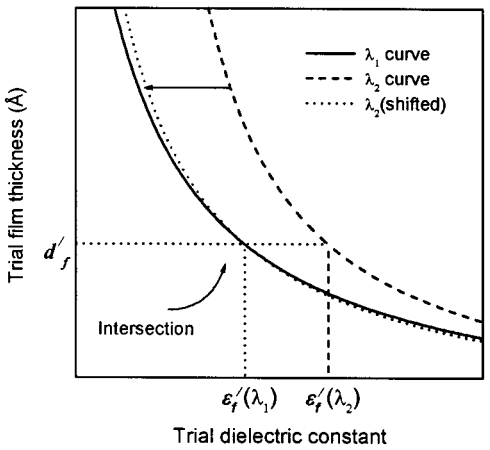

Figure 2. Illustration of the two-color SPR approach for determining thickness and dielectric constant for a thin film. We consider nonlinear least-squares fitting analysis of two different SPR reflectance curves obtained under identical experimental conditions except for excitation wavelength. The solid line shows all pairs of nonunique optical constants (d_f, ϵ_f) which equally well describe the SPR reflectance curve obtained at excitation wavelength λ_1; the dashed line shows all pairs of constants (d_f, ϵ_f) which equally well describe the SPR reflectance curve obtained at excitation wavelength λ_2. The unique thickness and dielectric constant of the film consistent with both data sets, shown graphically as the intersection point $\{d_f, \epsilon_f(\lambda_1)\}$, is found after accounting for the known dispersion of the thin film layer depicted here as the leftward shift of the trial curve for λ_2 (dotted line).

We and others have shown that unambiguous determination of the two unknown optical constants, the thickness, d_f, and dielectric constant, ϵ_f, for the unknown adsorbed film, can be achieved with either a two-color approach[8] or a multi-solvent approach.[9,20] The two-color method is more appropriate for measurements at solid/liquid interface as the processes of interest are likely to be solvent dependent. The methodology for two-color analysis has been shown both experimentally and theoretically.[8] Briefly, the analysis considers all possible combinations of d_f and ϵ_f that *equally well describe* the complete SPRS reflectance curve at a given excitation frequency. Each set of parameters defines a nonunique "best-fit" to the reflectance data. Sets of these best-fit parameters are compared for two different excitation wavelengths, and after accounting for the dispersion in all layers, a unique set of parameters for d_f and ϵ_f is found, Figure 2. These unique parameters self-consistently fit both complete SPR reflectance spectra obtained at both excitation wavelengths.

In this paper, SPRS optical data were analyzed as described previously[9] using nonlinear least-squares fitting to a multilayer Fresnel optical model. The analysis was performed using the Optimization Toolbox in MATLAB and adapted Fortran code originally supplied by Swalen (IBM). For the analysis, the optical constants for the prism and water were obtain from the literature while the dielectric constants for other solutions were obtained by measuring the critical angle in the appropriate solution using the SPRS apparatus.[21] All liquid dielectric constants were temperature corrected (values for d*n*/d*T* obtained from the literature or calculated from critical angle measurements). The average dielectric constants (at each wavelength) and average thickness for the gold and chromium layer were

(16) Otto, A. *Spectroscopy of Surface Polariton by Attenuated Total Reflection*; Otto, A., Ed.; North-Holland: Amsterdam, 1976; p 677.
(17) Pockrand, I.; Swalen, J. D.; Gordon, J. G.; Philpott, M. R. *Surf. Sci.* **1977**, *74*, 237−244.
(18) Gordon, J. G. I.; Swalen, J. D. *Opt. Commun.* **1977**, *22*, 374−376.
(19) Chinowsky, T. M.; Yee, S. S. *Sens. Actuators B* **1998**, *51*, 321−330.
(20) Bruijn, H. E. d.; Altenburg, B. S. F.; Kooyman, R. P. H.; Greve, J. *Opt. Commun.* **1991**, *82*, 425−432.
(21) Grassi, J. H.; Georgiadis, R. *Anal. Chem.* **1999**, *71*, 4392−4396.

calculated by optimizing the multilayer model parameters to fit the measured SPR spectra of piranha-cleaned gold in contact with water. The calculated gold layer thickness, which was within 8% of value measured by quartz crystal microbalance, was checked by optimizing the chromium and gold dielectric constants for a series of given gold thicknesses to fit the 543.5 nm spectra. Comparisons of the residuals, assuming a maximum optical signal error of 0.5% and a maximum position error of 0.001° for each measured reflectivity in the SPR spectrum, shows that the largest possible error in the average gold thickness determined by SPRS was ~2 Å. Details on the analysis procedure for determining surface coverage from dielectric constant data have been reported previously and are outlined in the next section. The signal to noise for our apparatus gives a maximum error in detecting ssDNA or HS-C_6-ssDNA of 0.7 ng/cm^2 (~1 fmol/mm^2, 0.5×10^{11} molecules/ cm^2).

2. Analysis of SPRS Kinetic Data. Figure 3 shows characteristic curves (coverage vs time) for several different models representing adsorption and desorption kinetics at solid/liquid interfaces. In theory, each of these models yields a characteristic unique adsorption/desorption isotherm; however, in practice, it can be difficult to test various kinetic models and to extract reliable kinetic parameters. High-quality data are needed over a wide range of surface coverage and time scale. Despite the emergence of a number of powerful surface analytical techniques, quantitation of absolute surface coverage at solid/solution interfaces remains a challenge.

We compared our adsorption and hybridization kinetic data with several existing kinetics models for adsorption isotherms, including

Langmuir adsorption

$$\frac{d\Gamma(t)}{dt} = k_a C_0\left(1 - \frac{\Gamma(t)}{\Gamma_{max}}\right) \quad (1)$$

Langmuir adsorption with first-order desorption

$$\frac{d\Gamma(t)}{dt} = k_a C_0\left(1 - \frac{\Gamma(t)}{\Gamma_{max}}\right) - k_d\Gamma(t) \quad (2)$$

second-order Langmuir adsorption

$$\frac{d\Gamma(t)}{dt} = k_a C_0\left(1 - \frac{\Gamma(t)}{\Gamma_{max}}\right)^2 \quad (3)$$

and random sequential adsorption (RSA)[22,23]

$$\frac{d\Gamma(t)}{dt} = k_a C_0\left[1 - 4\frac{\Gamma(t)}{\Gamma_{max}} + \frac{6\sqrt{3}}{\pi}\left(\frac{\Gamma(t)}{\Gamma_{max}}\right)^2 + 1.4069\left(\frac{\Gamma(t)}{\Gamma_{max}}\right)^3\right] - k_d\Gamma(t) \quad (4)$$

In addition, we developed a model that accounts for the three main physical processes at work at the solid/solution interface: mass transport through the solution, flux-dependent adsorption, and coverage-dependent desorption. Our adsorption/desorption/diffusion (ADD) model is described by coupled differential equations (eqs 5 and 6) using Fick's laws for mass transport of the adsorbate molecules in solution and a Langmuir adsorption/desorption model with a time-dependent flux:

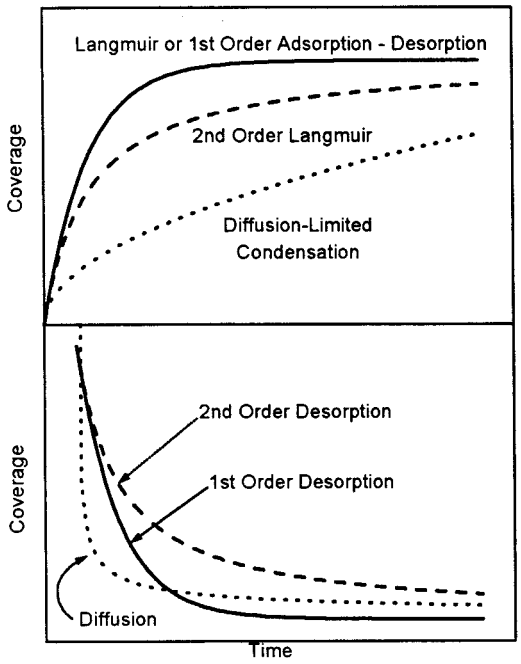

Figure 3. Illustration of typical coverage versus time curves for various selected models representing kinetic behavior for adsorption and desorption at the solid/liquid interface.

$$\frac{d\Gamma(t)}{dt} = J(t)\left(1 - \frac{\Gamma(t)}{\Gamma_{max}}\right) - k\Gamma(t) \quad (5)$$

$$J(t) = -D\frac{\partial c(x,t)}{\partial x}\bigg|_{\lim x \to 0} \quad (6)$$

Here, $\Gamma(t)$ is the time-dependent surface coverage for the adsorbed molecules (molecules/cm^2), Γ_{max} is the maximum possible coverage, c is concentration in solution (for these experiments ~1×10^{-5} g/cm^3 for HS-C_6-ssDNA), x is the distance from the flat surface, $J(t)$ is the time-dependent flux of (adsorbate) molecules into the surface, D is the diffusion constant for these molecules in solution, and k is the first-order desorption rate constant.

Kinetic modeling was implemented with custom-written C code. For our kinetic analyses, the procedure begins with the selection of a set of input parameters for the calculation. The coverage versus time curve is then calculated by solving the ADD model equations numerically, using a custom written C code. The calculated curve is compared to the experimental data and the process is repeated until a set of parameters is found which successfully describe the observed change in coverage as a function of time. The calculated coverage curve is constrained to match the measured coverage quantitatively over the time scale of the adsorption process while keeping the bulk solution concentration fixed at the experimental value.

The interdependence of the physical processes represented in the ADD model places extremely stringent constraints on the range of parameters, which can reasonably model a particular coverage vs time curve. More importantly, the resulting parameters can be interpreted directly in terms of physical processes at the interface, unlike the results from empirical fits.

4. Results

1. Overview: Formation and Characterization Nucleic Acid Monolayer Films. Surface plasmon resonance spectroscopy was used to follow the formation of the two-component

(22) Schaaf, P.; Talbot, J. *Phys. Rev. Lett.* **1989**, *62*, 175−178.
(23) Schaaf, P.; Talbot, J. *J. Chem. Phys.* **1989**, *91*, 4401−4409.

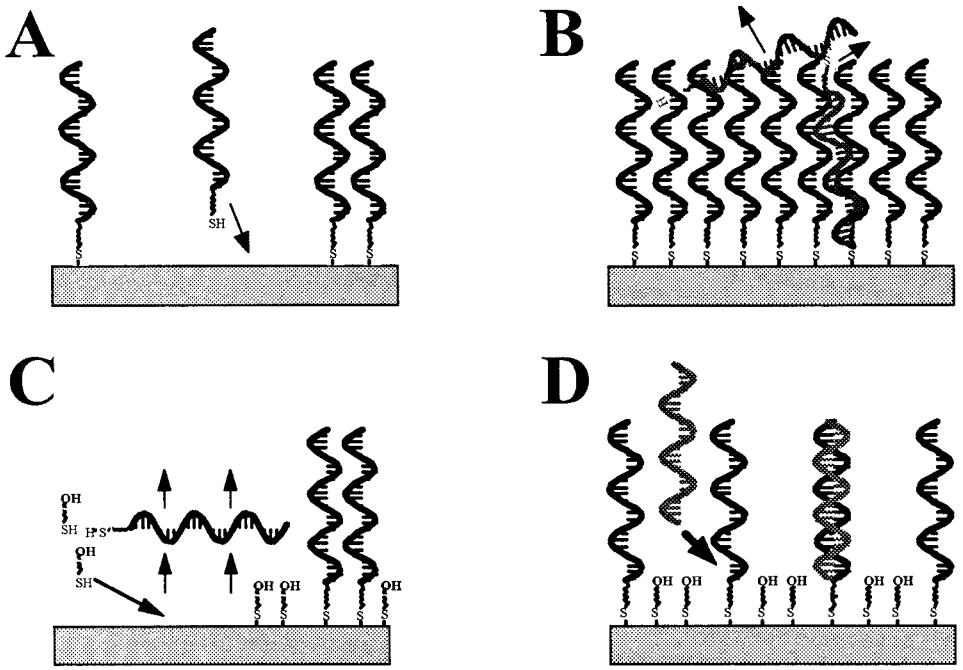

Figure 4. Schematic diagram indicating steps involved in the formation and hybridization of surface-tethered ssDNA films: (A) adsorption of HS-C_6-ssDNA on gold; (B) rinsing with water; (C) adsorption of mercaptohexanol and displacement of HS-C_6-ssDNA; and (D) hybridization of tethered ssDNA (black) with ssDNA complement (gray).

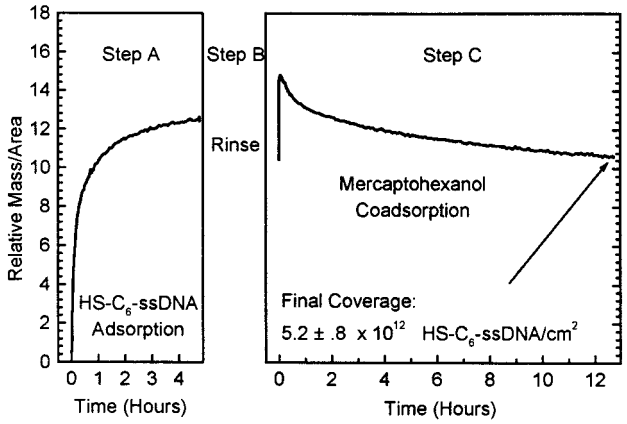

Figure 5. Kinetics of formation of a tethered ssDNA film measured by in situ two-color surface plasmon resonance spectroscopy. Shown is the relative mass/area versus time measured during the three-step process for forming a two-component film on gold. In step A the HS-C_6-ssDNA adsorbs on the gold surface. In step B, rinsing removes ~16% of the HS-C_6-ssDNA; and in step C, exposure to an aqueous solution of mercaptohexanol results in very rapid mercaptohexanol adsorption followed by slow desorption of HS-C_6-ssDNA. The final coverage of thiol-tethered DNA in the two-component film with mercaptohexanol diluent is $(5.2 \pm 0.8) \times 10^{12}$ HS-C_6-ssDNA/cm^2. Note that the abscissa refers to the mass per unit area for a single-component film in the left panel. The final coverage is calculated for ssDNA coverage in the two-component adsorbed film; see text for details.

film. The drawing in Figure 4 graphically illustrates the three steps for film formation: (A) adsorption of HS-C_6-ssDNA; (B) rinsing with water; and (C) coadsorption of mercaptohexanol with displacement of HS-C_6-ssDNA. The drawing in part D illustrates the process of hybridization of the tethered ssDNA film with the ssDNA complement.[10] Analysis of SPRS spectra collected during film formation, presented in Figure 5 as the relative mass of adsorbate molecules per unit area, confirms the basic steps involved in film formation. In step A, the mass/area increases, corresponding to adsorption of HS-C_6-ssDNA. In step B, the film is rinsed, and a 16% reduction in the total mass/area corresponds to loss of 16% of the HS-C_6-ssDNA. In step C, a rapid increase in mass/area corresponds to adsorption of mercaptohexanol. The slow decrease in mass/area corresponds to loss of previously adsorbed HS-C_6-ssDNA due to displacement.

Initial SPRS characterization of the surface hybridization process, step D, has been presented previously.[10] The importance of these studies is that they indicate that tethered ssDNA hybridizes with high efficiency with its complementary (unfunctionalized) ssDNA sequence. Furthermore, gold surfaces modified with a two-component thiol-ssDNA and mercaptohexanol film, illustrated in Figure 4D, appear to be resistant to nonspecific adsorption of ssDNA.

In subsequent sections, a detailed analysis of the two-color SPRS data is presented to quantify coverage and model kinetics for HS-C_6-ssDNA adsorption, mercaptohexanol mediated desorption of HS-C_6-ssDNA, and hybridization of surface-bound ssDNA stands to a fully complementary ssDNA, Figures 6, 7, and 8, respectively.

2. Quantitative Coverage by Two-Color SPRS:HS-C_6-ssDNA Adsorption. Procedures for determining surface coverage from refractive index data and the general application of the Clausius−Mossotti equation have been described in detail elsewhere.[8,9] Specific details for the DNA films used in the studies have been presented elsewhere.[10] The coverage of tethered ssDNA in the two-component film calculated from our SPRS data is $5.2 \pm 0.8 \times 10^{12}$ molecules/cm^2. This coverage is much less than the saturation coverage of small *n*-alkanethiols which are known to form monolayer films on gold (4.65×10^{14} molecules/cm^2). On the other hand, the maximum packing density of double-stranded DNA would correspond to $\sim 3 \times 10^{13}$ molecules/cm^2. Therefore, the DNA coverage in the two-component film is about one-fifth of the maximum possible coverage of a monolayer film. The coverage determined in our SPRS studies and previous hybridization efficiency results (calculated from coverage measurements) are in good agreement with complementary ex situ characterization and radio-labeling experiments.[24]

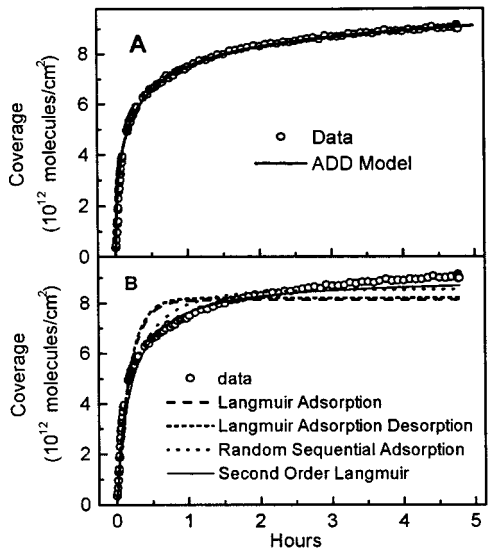

Figure 6. (A) Comparison of data for HS-C_6-ssDNA adsorption on gold with predictions of various models. Shown is the coverage versus time for the HS-C_6-ssDNA adsorption step (step A). The coverage is calculated from two-color SPR and the adsorption data are compared to those of a model that accounts for adsorption, desorption, and diffusion (ADD) of the adsorbate (see text). This model predicts a diffusion constant of 1.4×10^{-7} cm^2/s, a saturation coverage of $\sim 1 \times 10^{14}$ molecules/cm^2, and a desorption rate of 324 h^{-1} for the HS-C_6-ssDNA. (B) Comparisons of adsorption data to existing adsorption isotherm models (see text) which do not account for diffusion. All model curves are shown for best fit parameters. Although the second-order Langmuir model is closest to the adsorption data, none of the existing models fit the data as well as the ADD model.

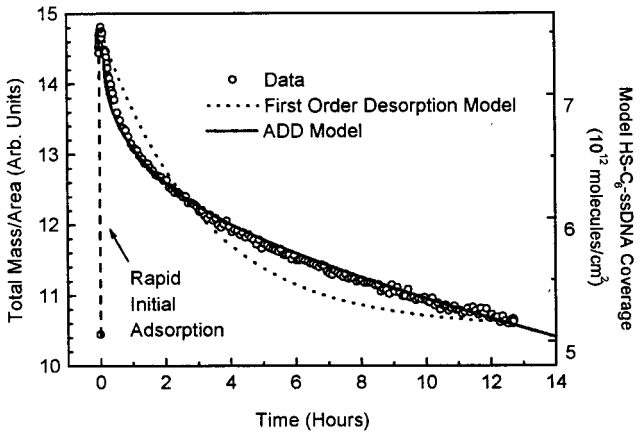

Figure 7. The kinetics of mercaptohexanol-mediated desorption of HS-C_6-ssDNA and quantitative comparison with models. The left axis refers to the total mass per unit area for the two-component film as measured by 2-color SPR. Through careful analysis of these data, in conjunction with other control experiments, the coverage of DNA is quantified. The desorption kinetics data are compared quantitatively to calculated models where the slow decrease in coverage is attributed solely to loss of HS-C_6-ssDNA (see text for details). The right axis refers to the coverage used in the model calculations. The mercaptohexanol-mediated desorption process is described well with the ADD model (solid line). The calculation predicts a diffusion constant of 1.4×10^{-7} cm^2/s and a desorption rate of 32 h^{-1} for the loss of HS-C_6-ssDNA. The same diffusion constant, 1.4×10^{-7} cm^2/s, was predicted by the ADD model for the *adsorption* kinetics of HS-C_6-ssDNA (Figure 6A). For completeness, the initial rapid adsorption of mercaptohexanol (dashed line) is shown. This process is comparable to the adsorption of mercaptohexanol on bare gold from aqueous solution in the rapid adsorption kinetics and in the measured coverage (to within about 20%).

3. Quantitative Coverage by Two-Color SPRS for a Two-Component Film: Mercaptohexanol Mediated Desorption. As shown in Figure 5 and in more detail in Figure 7, addition of a 1 mM mercaptohexanol solution to the sample cell produces a rapid increase in the amount of material on the surface followed by a long slow decrease. The increase in material is adsorption of mercaptohexanol, which is known to adsorb to gold to form self-assembled monolayer films.[25] Control experiments indicate that mercaptohexanol reaches a maximum coverage of $\sim 1.8 \times 10^{14}$ molecules/cm^2 when adsorbing onto bare gold from an aqueous solution. In these control experiments, the adsorption proceeded rapidly, and although there are too few data points for a detailed kinetic analysis, the data clearly show that the mercaptohexanol reaches and maintains a coverage of $\sim 1.4 \times 10^{14}$ molecules/cm^2 in less than 50 s. The mercaptohexanol adsorption on the HS-C_6-ssDNA/Au film reaches and maintains a coverage of $\sim 1.8 \times 10^{14}$ molecules/cm^2 in less than 50 s (Figure 7, dashed line). The presence of the previously adsorbed HS-C_6-ssDNA has little measurable effect on mercaptohexanol adsorption.

The long, slow loss of material from the surface is attributed to displacement of the HS-C_6-ssDNA by mercaptohexanol rather than loss of mercaptohexanol**.** This is reasonable for several reasons. Keeping in mind that the coverage of mercaptohexanol (1.8×10^{14} molecules/cm^2) is much greater than that of HS-C_6-ssDNA ($<7.6 \times 10^{12}$ molecules/cm^2), it is clear that loss of large amounts of mercaptohexanol would leave much of the gold surface bare. Such a surface would be conducive to nonspecific adsorption of DNA. In control experiments, no nonspecific adsorption of ssDNA is observed onto this surface[10] whereas significant adsorption is observed when ssDNA is presented to bare gold. *Ex situ* experiments also support the premise of mercaptohexanol mediated desorption of thiol-DNA. XPS measurements of the HS-C_6-ssDNA/Au film before and after exposure to mercaptohexanol show a decrease in the N 1s peak, clearly indicating loss of the HS-C_6-ssDNA.[24] Finally, SPR control experiments show that mercaptohexanol exposure leads to displacement of adsorbed ssDNA oligomer.

5. Discussion

1. Adsorption. Figure 6, parts A and B, shows the comparison of data for HS-C_6-ssDNA adsorption on gold (step A) with predictions of various models. The coverage is calculated from two-color SPR. In Figure 6A adsorption data are compared quantitatively with the model, which accounts for adsorption, desorption, and diffusion (ADD) of the adsorbate. This model predicts a diffusion constant of 1.4×10^{-7} cm^2/s, a saturation coverage of $\sim 1 \times 10^{14}$ molecules/cm^2, and a desorption rate of 324 h^{-1} for the HS-C_6-ssDNA.

Model curves which did not include both adsorption and desorption did not describe the data well, Figure 6B. All model curves are shown for best-fit parameters. Although the second-order Langmuir model is closest to the adsorption data, none of the existing models fits the data as well as the ADD model.

2. Kinetics of Mercaptohexanol-Mediated Desorption. Figure 7 shows the kinetics of desorption for the HS-C_6-ssDNA. These data were compared to several displacement and desorption models, including first-order desorption (dotted line in Figure 7), second-order desorption, and simple diffusion away from the surface (not shown). None of these models are adequate to account for the data.

(24) Herne, T. M.; Tarlov, M. J. *J. Am. Chem. Soc.* **1997**, *119*, 8916−8920.

(25) Poirier, G. E.; Tarlov, M. J.; Rushmeier, H. E. *Langmuir* **1994**, *10*, 3383−3386.

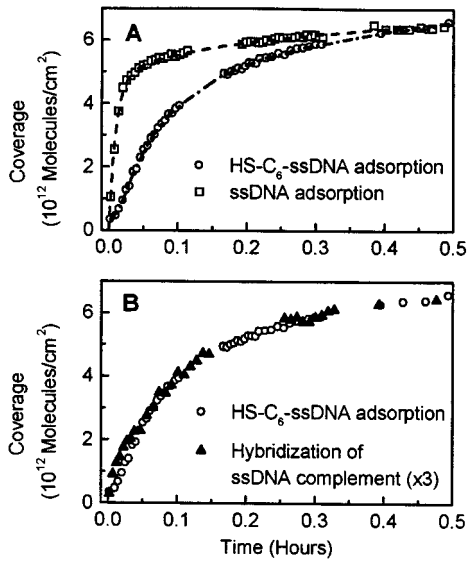

Figure 8. (A) The effect of the thiol modification to the kinetics of adsorption on bare gold. Shown are the kinetics of adsorption of ssDNA (open squares) and of HS-C_6-ssDNA (open circles) under the same conditions. Coverage is measured using in situ two-color SPR under the same experimental conditions. Note that the adsorption of HS-C_6-ssDNA can be described by a single kinetic step using the ADD model (solid line in Figure 6A). In contrast, a single kinetic step cannot account for the behavior of ssDNA adsorption (dotted line). See text for details. (B) Comparison of the kinetics of surface-confined hybridization (closed triangles) with the adsorption of HS-C_6-ssDNA on bare gold (open circles, same data as in part A). For the hybridization kinetics, the data (closed triangles) correspond to the amount of DNA that hybridizes to the surface-immobilized single-stranded DNA of fully complementary sequence. Hybridization is confirmed by in situ temperature-dependent SPR measurements which show that the de-hybridization temperature for the resulting surface immobilized duplex is only slightly depressed from the value for the same duplex in free solution. Control experiments show no nonspecific adsorption. Note that the hybridization coverage is scaled by a factor of 3. This scaling factor correctly accounts for loss of some adsorbed HS-C_6-ssDNA during rinsing and during mercaptohexanol-mediated desorption as well as for the efficiency of hybridization

The model which best describes the displacement and desorption of HS-C_6-ssDNA rigorously accounts for diffusion of the desorbed DNA away from the interface and allows for readsorption of HS-C6-ssDNA. The curve that best described the data, shown as a solid line in Figure 7, was calculated using an initial coverage of HS-C_6-ssDNA equal to $\Gamma(t=0) = 7.56 \times 10^{12}$ molecules/cm^2, the initial bulk solution concentration of thiol-modified ssDNA is zero, $D = 1.4 \times 10^{-7}$ cm^2/s, and $k = 32$ h^{-1}. It is striking that the kinetics of mercaptohexanol-mediated desorption of HS-C_6-ssDNA can be described using the same physical model (eqs 5 and 6) used to describe the kinetics of *adsorption* (Figure 6A). Furthermore, the parameters describing the two processes are self-consistent. The initial coverage used in the analysis of the desorption process is the same as the final coverage (after rinsing) of the adsorbed HS-C_6-ssDNA. The same diffusion constant for HS-C_6-ssDNA comes out of the kinetic analysis for both adsorption and desorption data.

It is not surprising that the calculated desorption rate constant for the mercaptohexanol displacement step (32/h) is different than that obtained for the thiol-DNA adsorbing to the bare gold (324/h) (see the previous section). The presence of a small but measurable amount to mercaptohexanol is likely to have a profound effect on the nature of the DNA surface interactions. Note also that in the mercaptohexanol mediated case, prior rinsing had removed a substantial fraction of weakly bound thiol-DNA (about 16%).

We note that our interpretation assumes that the observed change in mass/area is attributed exclusively to loss of HS-C_6-ssDNA. In other words, while there may be some additional mercaptohexanol adsorption after the initial rapid process, we assume that this contributes negligibly to the observed desorption data. The molecular weight of the mercaptohexanol (134.24) is almost two orders of magnitude less than the molecular weight of the HS-C_6-ssDNA (~8000). Assuming a 1:1 exchange, the contribution to the SPR data from the adsorbing mercaptohexanol would be less than 1.7% of the signal from the desorbing HS-C_6-ssDNA.

3. DNA Oligomer Adsorption: Effect of Thiol Functionalization on Adsorption Kinetics. In this section, we compare the kinetics of adsorption for two single-stranded DNA 25-mers of identical sequence, one of which is functionalized with a pendant *n*-$C_6H_{12}SH$ at the 5′ position. We will refer to the functionalized oligomer as HS-C_6-ssDNA and will refer to the unmodified single-stranded DNA 25-mer as ssDNA.

Figure 8A shows a comparison of the kinetics of adsorption for ssDNA and HS-C_6-ssDNA adsorption onto bare gold. Coverage versus time data, measured by *in situ* two-color SPR, are shown after exposure of a clean gold surface to a 0.5 μM solution of the oligomer in 1 M KH_2PO_4. For clarity, only the first 30 min of the adsorption process are shown; however, the best fits lines were calculated from analysis of the adsorption kinetics data measured over a 5-h period. For the adsorption of HS-C_6-ssDNA, the kinetics of adsorption are best modeled with the ADD model in a *single kinetic step* involving simultaneous adsorption, desorption, and diffusion (solid line in Figure 6A). In contrast, the adsorption of ss-DNA is very complex and cannot be modeled by a single kinetic step regardless of which model was considered. Preliminary analysis reveals that several kinetic steps must be invoked. The dotted line in Figure 8A shows the results of fitting the data to a model that includes three concerted steps consisting of (Step 1) Langmuir adsorption, (Step 2) adsorption, desorption, and diffusion (ADD), and (Step 3) condensation. These three kinetic steps are concerted: the condensation in Step 3 is proportional to coverage in Step 2, which in turn is related to the coverage in Step 1.

The overall kinetics of adsorption of HS-C_6-ssDNA on bare gold, although ultimately constrained to bind primarily through a single gold−thiol bond, include a measurable rate of desorption. In contrast, adsorption of ssDNA oligomer on bare gold, which binds through unconstrained nonspecific interactions, shows overall kinetics that are much faster, initially, presumably because the desorption rate is so low. This dramatic difference in kinetic behavior suggests that addition of a thiol functionality effects some of the nonspecific interactions. There may be other explanations for the behavior. One possibility we have explored and ruled out is related to the possibility of disulfide formation in the solution. The difference in the diffusion constant for DNA disulfide as compared to thiol-DNA is sufficient to alter the kinetics. Control experiments performed with solutions containing an excess (80 μM) of tris(2-carboxyethyl) phosphine, hydrochloride (TCEP), a compound used for fast quantitative and specific reduction of disulfide bonds and maintaining monothiols in a reduced state,[26] show no difference in kinetics. We confirmed experimentally that TCEP does not adsorb to the bare gold surface in DNA-free solution and therefore the presence of TCEP should not affect the kinetics of DNA adsorption.

(26) Burns, J. A.; Butler, J. C.; Moran, J.; Whitesides, G. M. *J. Org. Chem.* **1991**, *56*, 2648−50.

4. Hybridization Kinetics at Surface-Tethered DNA. In another set of experiments, a monolayer film of tethered ssDNA (HS-C_6-ssDNA/Au with co-adsorbed mercaptohexanol) is exposed to ssDNA oligomers of fully complementary sequence (Step D in Figure 4) and the complement is observed to adsorb. In contrast, when the fully noncomplementary sequence is used, no adsorption is measured. These control experiments indicate the absence of nonspecific binding and suggest the occurrence of sequence-specific hybridization, which we have confirmed through SPRS melting studies.[10] A direct comparison of the adsorption of HS-C_6-ssDNA and the hybridization of the ssDNA complement (scaled by a factor of 3) in panel B of Figure 8 shows a remarkable similarity between the kinetics for these two different, interfacial binding processes. The kinetics of ssDNA hybridization, that is, the adsorption of ssDNA constrained to form specific bonds to tethered ssDNA through formation of the double helix (Figure 8B, triangles), is in stark contrast to the kinetics of nonspecific adsorption of ssDNA on bare gold (Figure 8B, squares). Preliminary investigations indicate that the oligomer sequence mismatch and length strongly affect the kinetics of hybridization.[27]

We find that the kinetic data in this work deviate from the predictions of various constant flux models including simple Langmuir but can be fit self-consistently using the ADD model. That is, the kinetics cannot be understood without assuming a dynamic equilibrium, which takes into account adsorption and desorption as well as diffusion at the interface. The applicability of the ADD model has been observed in our laboratory for a variety of interfacial reactions. This behavior is also reported in the literature, for example, in the kinetics of highly selective antigen−antibody interactions at interfaces.[28] The contribution of dynamic equilibrium has implications for both fundamental and applied research; however, it has not been invoked in studies of self-assembly of alkanethiol monolayer films, except in very few studies.[29,30] Nevertheless, the mechanism of formation of even the simplext *n*-alkanethiol monolayer films at the gold/solution interface remains a subject of controversy.[31]

6. Conclusions

In this paper, we have presented a quantitative study of the formation and hybridization of a two-component tethered ssDNA film and show that each kinetic step leading to formation of the two-component film can be modeled quantitatively with a simple physical model that accounts for simultaneous adsorption, desorption, and diffusion of the adsorbate molecule. Kinetic parameters, such as the diffusion constant and desorption rate constant, can provide useful physical insights. For example, while most researchers who utilize self-assembled monolayer techniques assume implicitly or explicitly that there is no measurable desorption rate, our results indicate that the kinetics of self assembly of thiol-ssDNA cannot be understood without including both desorption and diffusion. The stringency of constraints placed on the parameters by our model (solutions of the differential equations for adsorption, desorption, and diffusion) as well as self-consistency of parameters between data sets increase our confidence in the analysis results.

We find a sharp contrast in the kinetics of surface-confined DNA hybridization, that is, the adsorption and binding of complementary ssDNA to a surface-tethered oligomer, compared with adsorption of the same ssDNA onto bare gold. This contrast is not surprising given that complementary DNA−DNA interactions leading to hybridization are likely to be far more constrained than nonspecific adsorption of single strands. We find that hybridization kinetics can be fit with a single step model that must include desorption, whereas nonspecific adsorption of ssDNA on bare gold shows complex behavior involving multiple kinetic steps and appears to have a negligible desorption rate constant.

Kinetic isotherms from quantitative SPRS are clearly useful for distinguishing between different types of adsorbate/surface interactions, such as constrained versus nonspecific interactions; however, further work is needed to more fully interpret the data. For example, we observe an apparent similarity in kinetic behavior for HS-C_6-ssDNA adsorption on bare gold, a process ultimately constrained to bind primarily through a single gold−thiol bond, and the binding of ssDNA to a surface-tethered ssDNA film of complementary sequence, a process constrained to form specific bonds through formation of the double helix. Both processes are similar in that they show kinetic behavior consistent with a single kinetic step involving adsorption, desorption, and diffusion in contrast with the complex behavior seen for nonspecific interactions of ssDNA on bare gold. However, additional work is underway to obtain a more complete understanding of these constrained interaction kinetics at interfaces.

Acknowledgment. Support is acknowledged from the National Science Foundation CAREER Award (Grant CHE-9502757) and NSF Career Advancement Award (Grant CHE9709347).

JA9930824

(27) Georgiadis, R.; Peterson, A. W.; Heaton, R. H. Manuscript in preparation.

(28) Rahn, J. R.; Hallock, R. B. *Langmuir* **1995**, *11*, 650−654.

(29) Karpovich, D. S.; Blanchard, G. J. *Langmuir* **1994**, *10*, 3315−3322.

(30) Schessler, H. M.; Karpovich, D. S.; Blanchard, G. J. *J. Am. Chem. Soc.* **1996**, *118*, 9645−9651.

(31) Dannenberger, O. B. M.; Grunze, M. *J. Chem. Phys. B* **1999**, *103*, 2202−2213.